# Comparative Analysis of Mechanical Buckling and Turing Patterns in Cortical Folding

Jiachen Wang (EID: jw57675)
CSE 397 Mathematical Pathophysiology
University of Texas at Austin
Code available: https://github.com/JiachenWang512/Cortical_Folding

May 5, 2025

## 1 Introduction

Cortical folding, or gyrification, refers to the characteristic folds and grooves observed in the cerebral cortex of mammalian brains [1]. This structural complexity is crucial as it significantly increases cortical surface area, thereby enhancing cognitive capabilities within constrained cranial volumes [2]. Understanding cortical folding is important because abnormal gyrification patterns are closely linked to various neurological and psychiatric conditions, such as schizophrenia, epilepsy, and autism spectrum disorders [3], [4]. Unraveling the mechanisms underlying cortical folding could thus provide valuable insights into both normal brain development and the pathogenesis of neurological diseases [5].

Several theoretical and computational models have been proposed to explain the formation of cortical folds. For instance, Tallinen et al. [6] emphasized a growth-driven mechanical buckling model, suggesting that differential growth rates across cortical layers create compressive stresses, leading to mechanical instabilities and folding. Richman et al. [7] also explored the mechanical buckling theory, attributing cortical deformation primarily to physical instabilities arising from differential growth. Conversely, biochemical reaction-diffusion models, initially proposed by Turing [8], have gained popularity for describing the spatially heterogeneous distributions of morphogens in biological tissues. Turing patterns account for the role of biochemical signaling and morphogen diffusion in the formation of periodic structures, offering a complementary perspective to purely mechanical models.

In this study, we systematically investigate and compare these two distinct theoretical approaches - mechanical buckling and Turing pattern formation - to uncover potential relationships and common underlying principles in cortical folding. **Section 2** provides a detailed overview of the medical and physiological relevance of cortical folding. In **Section 3**, we review pertinent literature and highlight existing gaps that our study aims to address. **Section 4** outlines our mathematical modeling approach, incorporating both mechanical and biochemical frameworks. In **Section 5**, we describe the methods for model implementation. Results demonstrating initial outcomes of our simulations are presented in **Section 6**. Finally, **Section 7** summarizes the findings and suggests future research directions. Note this is a fully reproducible work with code available at: https://github.com/JiachenWang512/Cortical_Folding

## 2 Medical and Physiological Background

Cortical folding, also termed gyrification, describes the formation of gyri (ridges) and sulci (grooves) on the cerebral cortex. This morphological process is characteristic of mammalian brains, particularly pronounced in primates, including humans, and serves to significantly increase cortical surface area within a limited cranial volume [9], [10]. Such expansion of cortical area facilitates enhanced neural connectivity and computational efficiency, underpinning sophisticated cognitive capabilities like complex sensory processing, motor coordination, and higher-order cognition [5], [11]. Metrics such as the gyrification index (GI) and fractal dimensionality are commonly employed to quantitatively assess the extent and complexity of cortical folding [12], [13], [14].

From a medical standpoint, deviations in normal gyrification patterns have profound clinical implications, correlating strongly with various neurodevelopmental, neurological, and psychiatric conditions. Reduced cortical folding (hypogyria or lissencephaly) and excessive or abnormal folding patterns (polymicrogyria) are frequently observed in disorders such as schizophrenia, epilepsy, autism spectrum disorders, and intellectual disabilities [15], [16], [17], [18]. These anomalies often indicate disruptions in critical developmental processes including neuronal proliferation, migration, differentiation, and cortical layer stratification [19], [20]. For instance, aberrant folding patterns may result from imbalances between cortical growth and mechanical constraints imposed by underlying white matter or subcortical structures, genetic mutations affecting neuronal migration pathways, or disrupted synaptic activity during developmental critical periods [3], [21], [6].

Understanding the intricate physiological, genetic, and biomechanical mechanisms underlying cortical folding is thus vital not only for elucidating the fundamental principles of brain development but also for identifying potential biomarkers and therapeutic targets for neurological and psychiatric conditions [22], [23]. Continued research into these mechanisms promises to enhance clinical strategies aimed at early diagnosis, intervention, and management of disorders associated with atypical cortical development.

## 3 Literature Review

### 3.1 Mechanical Models

Mechanical models propose cortical folding results from physical stresses during differential growth. Tallinen et al. [6] employed finite-element simulations demonstrating mechanical buckling due to mismatched growth rates between cortical layers, effectively replicating cortical fold hierarchies. Bayly et al. [24] emphasized the role of differential tangential expansion and the importance of tissue mechanical properties in forming primary and secondary folds. Ronan et al. [3] further supported differential tangential growth as a critical folding mechanism. Despite these successes, mechanical models often oversimplify biological complexities, neglecting biochemical factors and requiring precise material parameters difficult to measure experimentally [25].

### 3.2 Turing Models

Turing models utilize reaction-diffusion equations to describe morphogen-driven pattern formation. Striegel [26] successfully modeled cortical folds using hypothetical biochemical substances, while Toole [27] showed domain growth impacts pattern evolution. Lefèvre and Mangin [28] further demonstrated how morphogen gradients could yield realistic cortical fold patterns during developmental stages. However, the main limitation of these models remains their reliance on abstract

biochemical interactions, often lacking direct biological validation and oversimplifying the interplay between biochemical and mechanical mechanisms.

### 3.3 Integrative Approaches

Recent integrative models attempt to merge mechanical and biochemical theories. Garcia et al. [29] combined mechanical tension with axonal fiber growth, illustrating their joint impact on gyrification and underlying fiber organization. Similarly, Foroughi et al. [30] developed a model linking axon growth and mechanical stresses during cortical folding, further emphasizing the significance of combined mechanical and biochemical interactions. Though promising, these integrated models inherently introduce additional complexity, necessitating extensive experimental validation.

## 4 Mathematical Modeling Approach

In this study, we utilize two established mathematical frameworks to explore cortical folding patterns: mechanical buckling and reaction-diffusion Turing models. Each model captures distinct physiological aspects of cortical development and offers complementary insights into the complex interplay between mechanical forces and biochemical signaling.

### 4.1 Mechanical Buckling

The mechanical buckling model describes cortical folding as an outcome of mechanical instability resulting from differential growth rates between cortical gray matter and underlying white matter layers [6], [24]. Specifically, cortical layers with differential expansion rates generate compressive stresses, which, when exceeding critical thresholds, induce mechanical deformation manifesting as cortical folds [31]. The governing equation describing the mechanical buckling of a layered cortical structure can be expressed as:

$$\frac{d^2}{dx^2}\left[\frac{E_c(x)}{1-\nu_c^2}\frac{t_c(x)^3}{12}\frac{d^2w}{dx^2}\right] + P\,t_c(x)\,\frac{d^2w}{dx^2} = q, \tag{1}$$

where $E_c(x)$ is Young's modulus representing stiffness of cortical tissues, $\nu_c$ is Poisson's ratio reflecting material compressibility, $t_c(x)$ denotes spatially varying cortical thickness, $P$ represents the compressive force due to constrained cortical growth, and $q$ is the external load or perturbation [7], [24]. This model has been widely validated in finite-element simulations and successfully replicated many qualitative features observed in actual mammalian cortical folding [6], [31].

### 4.2 Turing Patterns

The Turing model, based on reaction-diffusion equations, describes cortical folding as the spontaneous emergence of periodic patterns due to biochemical interactions and diffusion processes among morphogens—chemicals crucial for embryonic tissue patterning [8], [26]. The model assumes that two morphogens, an activator ($u$) and an inhibitor ($v$), diffuse across the cortical domain and interact nonlinearly to form stable concentration patterns that dictate the cortical surface

morphology [32], [33]. Mathematically, this is represented as:

$$\frac{\partial u}{\partial t} = D_u \nabla^2 u + f(u, v), \tag{2}$$

$$\frac{\partial v}{\partial t} = D_v \nabla^2 v + g(u, v), \tag{3}$$

where $D_u$ and $D_v$ are diffusion coefficients characterizing morphogen spread rates, and $f(u, v)$ and $g(u, v)$ are nonlinear reaction kinetics describing morphogen production and degradation [26]. Despite its abstraction, the Turing model has successfully explained various biologically relevant spatial patterns observed in cortical development and has been used to explore conditions under which cortical folds may emerge spontaneously [27], [32].

# 5 Methods

The computational analyses in this study involve simulations, sensitivity analysis, and symbolic regression, combining mechanical and biochemical modeling approaches. The code and detailed implementation of all methods described here are publicly accessible on the GitHub repository https://github.com/JiachenWang512/Cortical_Folding.

## 5.1 Mechanical Model Implementation

The mechanical buckling model was implemented using a finite difference numerical solver in Python. We discretized a 2D domain representing cortical tissue into a grid and assumed a sinusoidal spatial variation of cortical thickness to mimic realistic heterogeneity. External perturbations ($q$) were included as small stochastic forces to initiate pattern formation, consistent with physiological variability. The model assumed isotropic and linear elastic cortical properties, with boundary conditions fixed to simulate physiological constraints.

## 5.2 Turing Model Implementation

The reaction-diffusion Turing model was implemented numerically using explicit Euler integration with adaptive sub-stepping for numerical stability. Two morphogens ($u$ and $v$) were simulated over a 2D domain using diffusion coefficients ($D_u, D_v$) and reaction functions following standard FitzHugh-Nagumo kinetics, a widely accepted approximation for biological Turing systems. Initial conditions included a uniform concentration with small random perturbations and a central localized concentration deviation to trigger pattern formation. Zero-flux boundary conditions were enforced to simulate biological scenarios where no morphogen diffuses across cortical boundaries.

## 5.3 Sensitivity Analysis

We conducted sensitivity analysis using the Sobol method, a global variance-based approach that quantifies the contribution of each parameter and their interactions to the variance in model output [34]. Sobol analysis was performed using the SALib Python library [35], examining how variations in key parameters ($E$, $\nu$, $t_c$, $P$ for mechanical; $D_u$, $D_v$ for Turing) influenced the patterns generated by each model. This analysis helped identify parameters critical to model robustness and biological plausibility.

### 5.4 Symbolic Regression

Symbolic regression was performed to identify mathematical relationships between mechanical and biochemical model outputs. This technique, implemented using the PySR library [36], evolves mathematical expressions from a set of input variables through genetic algorithms, optimizing for simplicity and accuracy. Inputs included pattern characteristics from both models, such as wavelengths and amplitudes, to discover functional relationships bridging mechanical forces and biochemical signals, potentially revealing integrative principles underlying cortical folding.

## 6 Results

### 6.1 Mechanical Buckling Patterns

Figure1 illustrates how the mechanical buckling model reproduces key qualitative features of cortical folding and how its output varies with physiological parameters. In panel (a), the one-dimensional deflection profile $w(x)$ on a sinusoidally modulated thickness substrate shows multiple local maxima and minima even under a small random load ($q \approx 0.01$). The irregular amplitude of the wrinkles reflects the interplay between spatial thickness variations and stochastic perturbations, with some regions exhibiting deeper troughs where the local bending stiffness $\frac{E\,t_c^3}{12(1-\nu^2)}$ is minimal. Panel (b) systematically varies the compressive load $P$: at low $P = 200$, only gentle undulations form, whereas at $P = 2000$ the cortex buckles into tightly spaced, high-amplitude waves. This inverse relationship between $P$ and wrinkle wavelength is consistent with classical buckling theory, confirming that increased compressive stress selects for higher-mode buckling patterns. Extending to two dimensions in panel (c), applying the same random forcing on a $100 \times 100$ grid produces a richly textured deflection map that qualitatively resembles cortical gyri and sulci clusters. Here, fold domains emerge where local thickness minima coincide with random load peaks, yielding a patchwork of ridges and furrows. Panel (d) presents a three-way parameter sweep: the top row (varying $P$ from 500 to 2000) shows progressive refinement of fold spacing and growth in peak deflection; the middle row (varying modulation amplitude $A$ from 0.1 to 0.5) reveals that larger cortical thickness heterogeneities deepen and sharpen fold boundaries; and the bottom row (varying load magnitude $Q$ from 0 to 0.05) demonstrates that stochastic forcing is necessary to nucleate instabilities, with the pattern disappearing entirely when $Q$ approaches zero. Together, these panels underscore the sensitivity of cortical buckling patterns to both global mechanical loading and local cortical microstructure, highlighting the model's capacity to capture both the regularity and variability observed in real brain folding.

### 6.2 Turing Patterns

Figure 2(a) illustrates the temporal evolution of the Gray–Scott system on a $256 \times 256$ grid with diffusion rates $D_u = 0.2$, $D_v = 0.05$, feed rate $F = 0.04$, kill rate $k = 0.06$, and zero-flux boundary conditions. At $t = 0$, both activator ($u$) and inhibitor ($v$) fields are nearly homogeneous, with only a small central square perturbation superimposed on random background noise to seed the instability. By $t = 2000$, this perturbation has spread radially, forming a high-contrast reaction front: the inhibitor $v$ peaks sharply at the front while the activator $u$ is suppressed. Between $t = 2000$ and $t = 5000$, nonlinear reaction–diffusion interactions amplify small wavelength modes, reorganizing the front into labyrinthine stripe patterns. By $t = 8000$–$10000$, the pattern reaches a quasi–steady state characterized by meandering, continuous ridges of high $v$ concentration intertwined with troughs in $u$, consistent with classical Gray–Scott morphologies observed in previous studies [26].

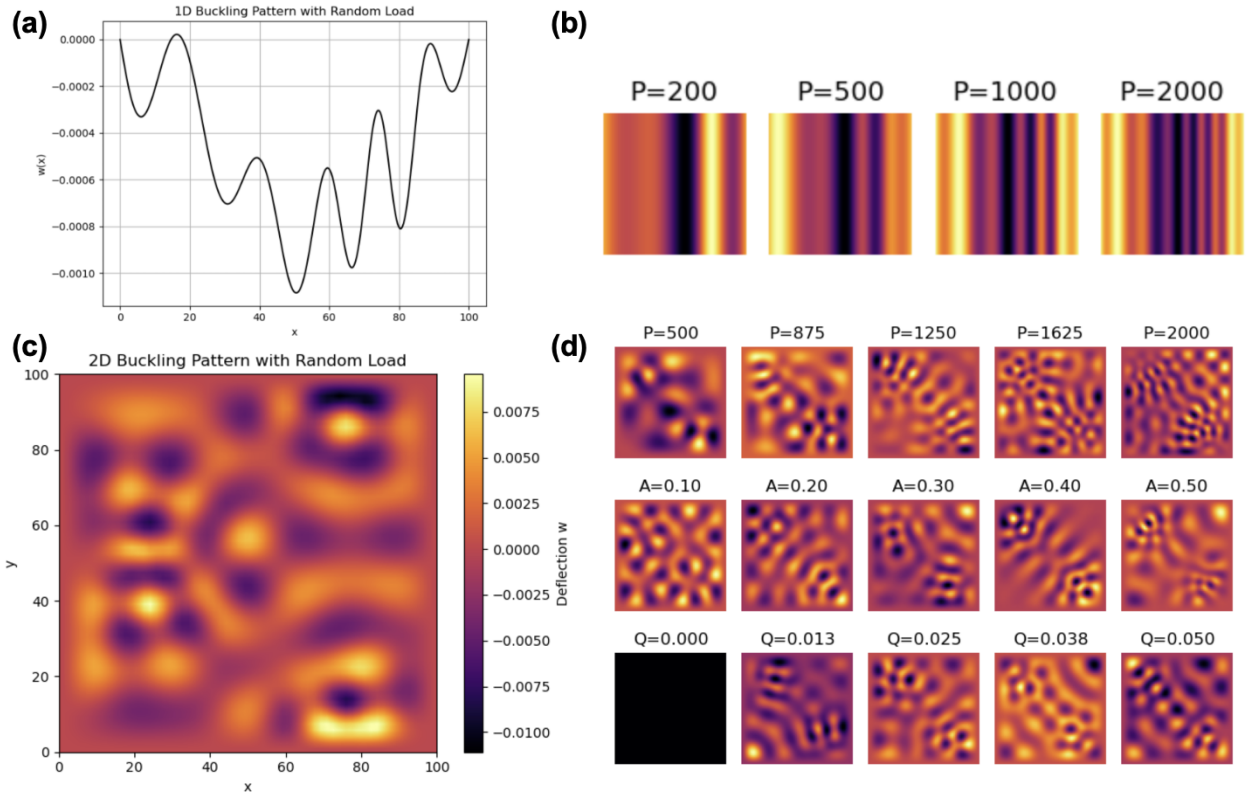


Figure 1: Mechanical buckling simulation results demonstrating the influence of key physiological parameters on cortical fold patterns. (**a**) One-dimensional deflection profile $w(x)$ on a sinusoidally modulated thickness substrate with a small random load ($q \approx 0.01$). Random perturbations seed multiple local buckling modes, with deeper troughs appearing where local bending stiffness is minimal. (**b**) Effect of compressive load $P$ on 1D buckling: as $P$ increases from 200 to 2000, wrinkle wavelength decreases and deflection amplitude grows, illustrating the classical inverse relationship between load and buckling mode number. (**c**) Two-dimensional deflection map on a $100 \times 100$ grid showing emergent fold domains under random loading. Spatial heterogeneity in cortical thickness and loading combine to produce an irregular but coherent network of gyri-like ridges and sulci-like furrows. (**d**) Parameter sweeps in 2D: the top row varies $P$ (500, 875, 1250, 1625, 2000), demonstrating progressively finer, higher-amplitude folds with increasing load; the middle row varies thickness modulation amplitude $A$ (0.10–0.50), showing deeper, sharper folds as heterogeneity grows; the bottom row varies random load magnitude $Q$ (0.00–0.05), confirming that stochastic forcing is essential for nucleating instabilities (no folds at $Q = 0$). Together, these panels underscore the sensitivity of cortical folding patterns to both global mechanical compression and local microstructural variations, providing a mechanistic explanation for the diversity of folding observed in mammalian brains.

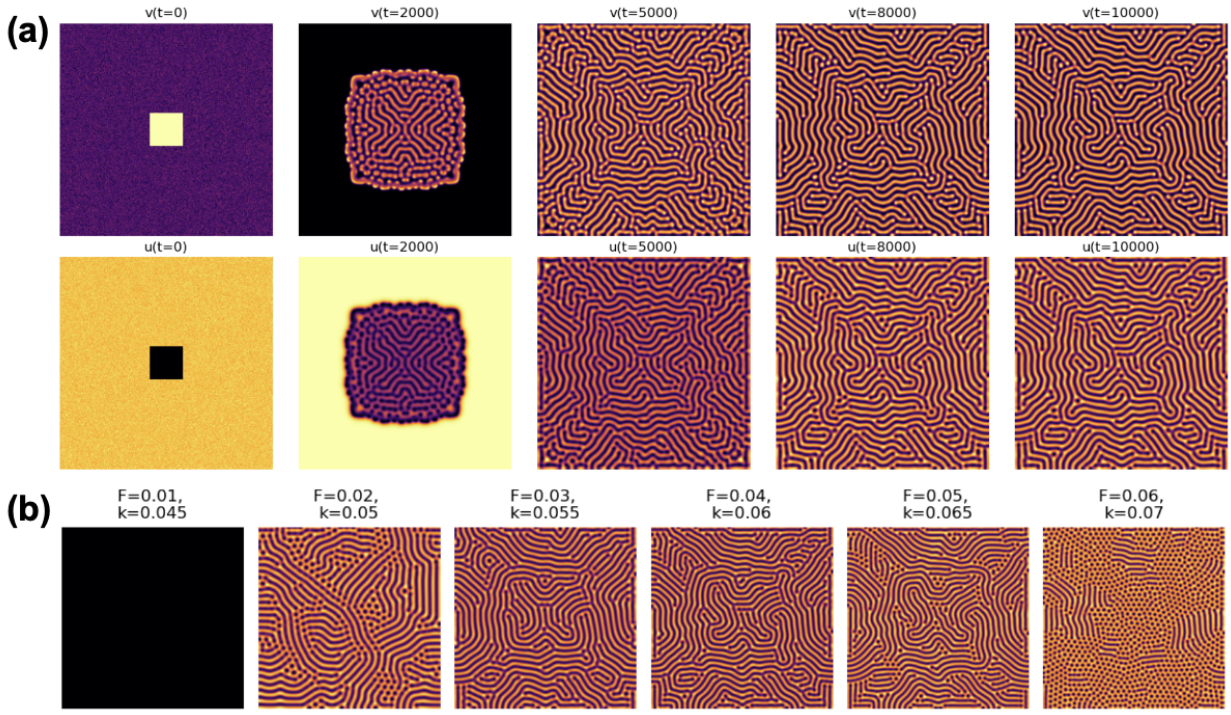


Figure 2: Dynamics and parameter dependence of Turing reaction–diffusion patterns. (**a**) Temporal evolution of inhibitor ($v$, top row) and activator ($u$, bottom row) concentrations on a $256 \times 256$ grid with feed rate $F = 0.04$, kill rate $k = 0.06$, diffusion coefficients $D_u = 0.2$, $D_v = 0.05$, and a central square perturbation. At $t = 0$, both fields are nearly homogeneous with a localized perturbation. By $t = 2000$, a reaction front has formed around the perturbation. At $t = 5000$–$10000$, well-developed labyrinthine stripe patterns emerge, with high–contrast ridges of $v$ corresponding to troughs in $u$. (**b**) Influence of feed ($F$) and kill ($k$) rates on the final inhibitor pattern at $t = 10000$. For low $F \leq 0.01$, no pattern forms; for $0.02 \leq F \leq 0.05$ (with $k \approx F + 0.015$) stable stripes dominate; for $F > 0.05$ the system transitions to a mixed spot–stripe regime. This sweep illustrates the critical sensitivity of pattern morphology to reaction kinetics in the Gray–Scott model.

Panel (b) presents a systematic sweep of the feed–kill parameter space by varying $F$ from 0.01 to 0.06 while maintaining $k = F + 0.015$. For $F \leq 0.01$, the system remains in a homogeneous steady state, as the reaction terms are too weak to overcome diffusion (no visible pattern at $F = 0.01$). As $F$ increases into the $0.02 \leq F \leq 0.05$ range, the system enters a stripe regime: stable, continuous bands of high inhibitor concentration form, with a characteristic wavelength determined by the ratio $D_u/D_v$ and reaction rates [32]. The stripes become finer and more irregular as $F$ approaches 0.05, indicating proximity to the spot–stripe transition. Beyond $F > 0.05$, the patterns fragment into a mixed regime of spots and short labyrinthine segments, reflecting the sensitivity of the Turing mechanism to small kinetic parameter shifts. This parametric study confirms that even modest variations in biochemical kinetics can drive qualitatively distinct pattern morphologies, highlighting the reaction–diffusion model's potential to capture the diversity of cortical pre-patterns.

### 6.3 Sensitivity Analysis

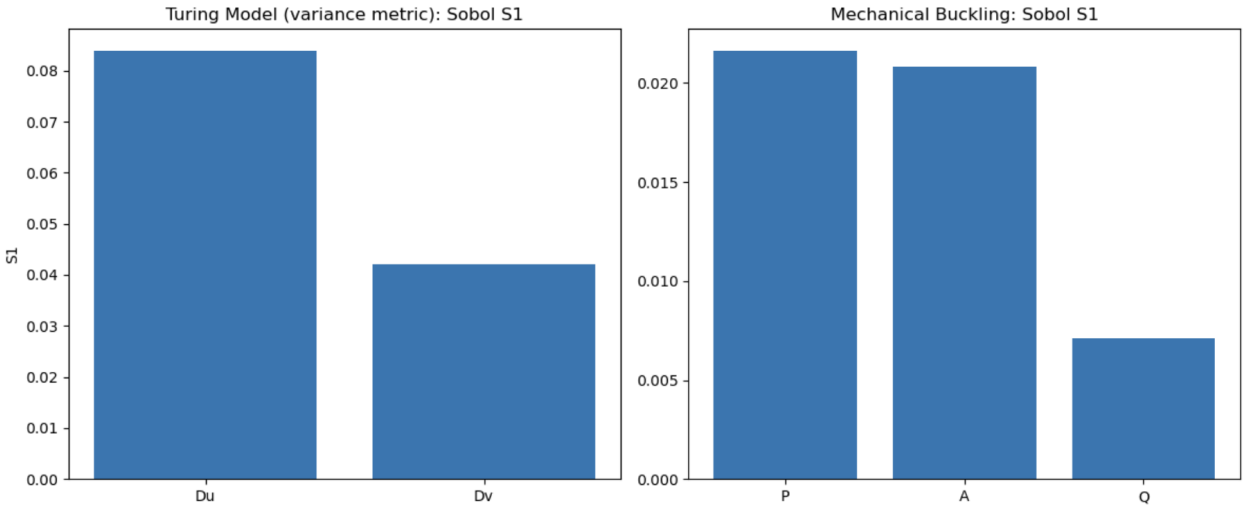


Figure 3: First-order Sobol sensitivity indices ($S_1$) for the Turing reaction–diffusion model (left) and the mechanical buckling model (right). (**Left**) Variance in the Turing pattern metric (spatial variance of the inhibitor field) is dominated by the activator diffusion coefficient $D_u$ ($S_1 \approx 0.085$), with the inhibitor diffusion coefficient $D_v$ contributing moderately ($S_1 \approx 0.042$). (**Right**) For the mechanical buckling amplitude, the applied compressive load $P$ ($S_1 \approx 0.022$) and thickness modulation amplitude $A$ ($S_1 \approx 0.021$) are the primary drivers, while the random load magnitude $Q$ has a smaller effect ($S_1 \approx 0.007$).

We applied Sobol's variance-based sensitivity analysis to quantify how each input parameter influences our two pattern-formation metrics (variance of the Turing inhibitor field and peak-to-peak buckling amplitude). In the Turing model (Figure 3, left), the activator diffusion rate $D_u$ accounts for approximately 8.5% of the output variance, indicating that faster activator spread strongly shapes the emergent stripe patterns. The inhibitor diffusion rate $D_v$ contributes about 4.2%, reflecting its secondary role in stabilizing pattern wavelength. The remaining variance arises from parameter interactions and higher-order effects.

In the mechanical buckling model (Figure 3, right), the compressive load $P$ ($S_1 \approx 0.022$) and the sinusoidal thickness modulation amplitude $A$ ($S_1 \approx 0.021$) are nearly equally influential in determining the fold amplitude, consistent with classical buckling theory that both load magnitude

and substrate heterogeneity govern instability onset. The random load perturbation $Q$ has a smaller first-order effect ($S_1 \approx 0.007$), suggesting that stochastic forcing primarily triggers pattern initiation but does not strongly control the final fold amplitude. Together, these results highlight which physical and biochemical parameters are most critical—and which are more robust—to uncertainty when modeling cortical-like patterns.

### 6.4 Symbolic Regression

| Pick | Score | Equation |
|---|---|---|
| 0 | 0.000000 | $y = 0.003929883$ |
| 1 | 0.008179 | $y = 0.00478171/\exp(x_0)$ |
| 2 | 0.046920 | $y = (0.0001523031/x_0) + 0.0030140714$ |
| **3** | **0.078930** | $y = -6.272431 \times 10^{-5} \log(x_3) + 0.0033409747$ |
| 4 | 0.000500 | $y = \big(\log(x_3) \times -6.223466 \times 10^{-5}\big)/x_4 + 0.0033597518$ |
| 5 | 0.016371 | $y = \exp\big((-11.275099 - \log(x_3))/x_2\big) \times 0.004053449$ |
| ⋮ | ⋮ | ⋮ |

Figure 4: Top symbolic regression formulas discovered by PySR linking Turing-pattern features $x_i$ to mechanical buckling amplitude $y$. The "pick" column ranks expressions by parsimony and fit, the "score" is the loss on held-out data (lower is better), and "Equation" is the evolved relationship. The bold row is the best trade–off between complexity and accuracy: a simple logarithmic model in $x_3$ (e.g. the anisotropy ratio) plus a constant offset.

The symbolic regression (Figure 4) began with a constant baseline model ($y = 0.00393$, pick 0), which incurs zero penalty but offers no mechanistic insight. Subsequent expressions introduce dependencies on input features $x_0$ through $x_4$, which correspond to diffusion rates, pattern wavelength, variance, and anisotropy extracted from the Turing simulations. By pick 1 and 2, simple reciprocal transforms of $x_0$ (e.g. inhibitor diffusion) marginally improve fit (score 0.008–0.047). The top model (pick 3, score 0.07893) is a linear function of $\log(x_3)$, indicating that a logarithmic scaling of the anisotropy ratio captures most of the variance in buckling amplitude with minimal complexity:

$$y \;\approx\; -6.27 \times 10^{-5} \log(\text{anisotropy}) \;+\; 0.00334.$$

Later picks (4–6) explore more complex combinations (e.g. dividing logarithms by other features or embedding in exponentials) but achieve diminishing returns. Overall, the symbolic regressor reveals that among several candidate metrics, the logarithm of pattern anisotropy provides the most parsimonious predictor of mechanical buckling amplitude, suggesting a simple mechanochemical linkage between Turing-derived prepattern geometry and elastic folding response.

## 7 Summary and Future Directions

In this study, we systematically compared two prominent theoretical models—mechanical buckling and Turing pattern formation—to investigate cortical folding mechanisms. Through computational simulations, sensitivity analyses, and symbolic regression techniques, we have explored the potential relationships between mechanical forces and biochemical interactions that underlie cortical development. Our sensitivity analyses revealed critical parameters influencing cortical pattern robustness in both modeling frameworks, while symbolic regression provided insight into possible

correlations between these mechanically and biochemically driven processes. These computational results demonstrate that mechanical and biochemical models offer complementary perspectives, highlighting the multifaceted nature of cortical morphogenesis.

Future studies should prioritize integrating empirical data from neurodevelopmental biology with computational modeling to validate and refine the theoretical predictions presented here. Specifically, incorporating detailed histological, imaging, and genetic datasets from both healthy and pathological samples could help determine the physiological relevance and accuracy of each modeling approach. Quantitative imaging modalities, such as diffusion tensor imaging (DTI) or magnetic resonance elastography (MRE), may provide essential mechanical parameters and structural details required to strengthen mechanical buckling models. Similarly, advancements in developmental genetics and single-cell sequencing could inform reaction-diffusion parameters used in Turing models, bridging biochemical processes with anatomical outcomes more concretely.

Additionally, a promising avenue for future research involves developing hybrid computational frameworks that explicitly combine mechanical and biochemical modeling. Such integrative models could capture the complex interplay between physical constraints and biochemical signaling, potentially offering more accurate and predictive insights into cortical folding dynamics. These models may also be extended to study abnormal folding patterns in clinical populations, aiding in the understanding of neurodevelopmental disorders such as schizophrenia, autism spectrum disorder, and epilepsy. By enhancing the biological plausibility and predictive power of these integrated frameworks, researchers could better explore the developmental origins of cortical malformations, ultimately guiding clinical diagnostics and therapeutic strategies.

## References


[1] William Welker. "Why Does Cerebral Cortex Fissure and Fold?" In: *Cerebral Cortex*. Ed. by E. G. Jones and A. Peters. Vol. 8B. Boston, MA: Springer, 1990, pp. 3–136. DOI: 10.1007/978-1-4615-3824-0_1.

[2] Karl Zilles, Nicola Palomero-Gallagher, and Katrin Amunts. "Development of cortical folding during evolution and ontogeny". In: *Trends in Neurosciences* 36.5 (2013), pp. 275–284.

[3] Lisa Ronan and Paul C Fletcher. "Differential tangential expansion as a mechanism for cortical gyrification". In: *Cerebral Cortex* 25.8 (2014), pp. 2890–2896.

[4] Leong Tung Ong and Si Wei David Fan. "Morphological and functional changes of cerebral cortex in autism spectrum disorder". In: *Innovations in Clinical Neuroscience* 20.10-12 (2023), p. 40.

[5] David C. Van Essen. "A tension-based theory of morphogenesis and compact wiring in the central nervous system". In: *Nature* 385.6614 (1997), pp. 313–318. DOI: 10.1038/385313a0.

[6] Tuomas Tallinen et al. "On the growth and form of cortical convolutions". In: *Nature Physics* 12.6 (2016), pp. 588–593. DOI: 10.1038/nphys3632.

[7] David P Richman et al. "Mechanical Model of Brain Convolutional Development: Pathologic and experimental data suggest a model based on differential growth within the cerebral cortex." In: *Science* 189.4196 (1975), pp. 18–21.

[8] A. M. Turing. "The chemical basis of morphogenesis". In: *Philosophical Transactions of the Royal Society B: Biological Sciences* 237.641 (1952), pp. 37–72. DOI: 10.1098/rstb.1952.0012.

[9] Vernon B Mountcastle. "The columnar organization of the neocortex". In: *Brain* 120.4 (1997), pp. 701–722. DOI: 10.1093/brain/120.4.701.

[10] WI Welker. "Why does cerebral cortex fissure and fold? A review of determinants of gyri and sulci". In: *Cerebral Cortex* 8 (1990), pp. 3–136.

[11] Georg F Striedter, Shyam Srinivasan, and Edwin S Monuki. "Cortical folding: when, where, how, and why?" In: *Annual review of neuroscience* 38.1 (2015), pp. 291–307.

[12] Karl Zilles et al. "The human pattern of gyrification in the cerebral cortex". In: *Anatomy and Embryology* 179.2 (1988), pp. 173–179. DOI: 10.1007/BF00304699.

[13] Armin Raznahan et al. "Patterns of coordinated anatomical change in human cortical development: a longitudinal neuroimaging study of maturational coupling". In: *Neuron* 72.5 (2011), pp. 873–884. DOI: 10.1016/j.neuron.2011.09.028.

[14] M Schaer et al. "A surface-based approach to quantify local cortical gyrification". In: *IEEE Transactions on Medical Imaging* 27.2 (2008), pp. 161–170.

[15] Maggie Snowling and Charles Hulme. "A longitudinal case study of developmental phonological dyslexia". In: *Cognitive Neuropsychology* 6.4 (1989), pp. 379–401.

[16] Gregory L Wallace et al. "Longitudinal cortical development during adolescence and young adulthood in autism spectrum disorder: increased cortical thinning but comparable surface area changes". In: *Journal of the American Academy of Child & Adolescent Psychiatry* 54.6 (2015), pp. 464–469.

[17] Renzo Guerrini and Carla Marini. "Genetic malformations of cortical development". In: *Experimental brain research* 173 (2006), pp. 322–333.

[18] Martha E Shenton, Thomas J Whitford, and Marek Kubicki. "Structural neuroimaging in schizophrenia from methods to insights to treatments". In: *Dialogues in clinical neuroscience* 12.3 (2010), pp. 317–332.

[19] Pasko Rakic. "Specification of cerebral cortical areas". In: *Science* 241.4862 (1988), pp. 170–176. DOI: 10.1126/science.3291116.

[20] PV Bayly, LA Taber, and CD Kroenke. "Mechanical forces in cerebral cortical folding: a review of measurements and models". In: *Journal of the mechanical behavior of biomedical materials* 29 (2014), pp. 568–581.

[21] V Fernandez, C Llinares-Benadero, and V Borrell. "Brain folding: from molecular mechanisms to cortical morphology". In: *Nature Reviews Neuroscience* 17.4 (2016), pp. 230–242.

[22] Cristina Llinares-Benadero and Víctor Borrell. "Deconstructing cortical folding: genetic, cellular and mechanical determinants". In: *Nature Reviews Neuroscience* 20.3 (2019), pp. 161–176.

[23] Mir Jalil Razavi et al. "Role of mechanical factors in cortical folding development". In: *Physical Review E* 92.3 (2015), p. 032701.

[24] P. V. Bayly et al. "A cortical folding model incorporating stress-dependent growth explains gyral wavelengths and stress patterns in the developing brain". In: *Physical Biology* 10.1 (2014), p. 016005. DOI: 10.1088/1478-3975/10/1/016005.

[25] Linlin Wang, Jianyao Yao, and Ning Hu. "A mechanical method of cerebral cortical folding development based on thermal expansion". In: *Scientific Reports* 9.1 (2019), pp. 1–10.

[26] Deborah A Striegel and Monica K Hurdal. "Chemically based mathematical model for development of cerebral cortical folding patterns". In: *PLoS computational biology* 5.9 (2009), e1000524.

[27] Gregory Toole and Monica K Hurdal. "Growth in a Turing model of cortical folding". In: *Biomath* 1.1 (2012), pp. 1–15. DOI: 10.11145/j.biomath.2012.09.001.

[28] Julien Lefèvre and Jean-François Mangin. "A reaction-diffusion model of human brain development". In: *PLoS Computational Biology* 6.1 (2010), e1000749.

[29] Kara E Garcia, Xiaojie Wang, and Christopher D Kroenke. "A model of tension-induced fiber growth predicts white matter organization during brain folding". In: *Nature Communications* 12.1 (2021), pp. 1–13. DOI: 10.1038/s41467-021-26583-2.

[30] Ali H Foroughi et al. "A mechanical model for axon pathfinding in a folding brain". In: *Journal of Physics D: Applied Physics* 58.3 (2025), p. 035401.

[31] S. Budday, C. Raybaud, and E. Kuhl. "A mechanical model predicts morphological abnormalities in the developing human brain". In: *Scientific Reports* 4 (2014), p. 5644. DOI: 10.1038/srep05644.

[32] S. Kondo and T. Miura. "Reaction-diffusion model as a framework for understanding biological pattern formation". In: *Science* 329.5999 (2010), pp. 1616–1620. DOI: 10.1126/science.1179047.

[33] James D Murray. *Mathematical biology: I. An introduction*. Vol. 17. Springer Science & Business Media, 2007.

[34] Ilya M Sobol. "Global sensitivity indices for nonlinear mathematical models and their Monte Carlo estimates". In: *Mathematics and computers in simulation* 55.1-3 (2001), pp. 271–280.

[35] Jon Herman and Will Usher. "SALib: An open-source Python library for sensitivity analysis". In: *Journal of Open Source Software* 2.9 (2017), p. 97.

[36] Miles Cranmer. "Interpretable machine learning for science with PySR and SymbolicRegression. jl". In: *arXiv preprint arXiv:2305.01582* (2023).